Brownian Dynamics of a Confined Circle Swimmer

B A C H E L O R A R B E I T

vorgelegt von

Urs Zimmermann

angefertigt am Institut für Theoretische Physik II
der Mathematisch-Naturwissenschaftlichen Fakultät
der Heinrich-Heine-Universität Düsseldorf

Düsseldorf, im Dezember 2008

Contents

Introduction

The science of *soft condensed matter* is a broad field of research discussing the physical states of systems such as colloids, polymers, foams, gels and granular or biological materials. All systems have in common that they can be easily manipulated by energies on the scale of the thermal energy at room temperature. For this reason, we often interact with soft condensed matter systems in our everyday life. Some of the numerous examples are food, soaps, shampoos, LCD-screens, ink, paints and – as a very complex system – the human being itself. The underlying structures that are analyzed are typically of a mesoscopic length-scale ranging from some nanometers to micrometers. At this length-scale the quantum nature of matter needs not to be taken into account since the size range of soft matter objects is much larger than the thermal de Broglie wavelength.

Recently research of so-called active particles has become of interest. Active particles are characterized by an internal, self-propelling force that drives these particles' motion. By definition, systems of active particles are out of equilibrium so many interesting effects such as giant diffusion [13], swarming [19] and swirling [12] occur. Although such kind of particles seem to be an artificial model at first glance, they have the potential to describe the dynamics of special systems such as self-propelling bacteria [1,4,11] or nano-rods [2]. There might also be some cases in which these mesoscopic models can be translated to macroscopic problems, for instance the motion of people on crowded streets [9] or in panic situations [10].

This Bachelor thesis focuses on a single self-propelled colloidal rod in two dimensions experiencing a constant force along its orientation and a constant torque, which alters its orientation. As this particle performs a circular trajectory in the absence of the disturbing influence of finite temperature effects, we will refer to it as a circle swimmer. In this thesis, we probe the dynamics of such a swimmer that is confined by different circular and ring-shaped potentials including, as well, finite temperature effects.

In nature we can find many examples of organisms that may be described by this model, for instance bacteria that are propelled by polymerization of actin:actin filaments [17] or spermatozoa [8, 20] that move in two dimensional confinement in circles. Moreover, man-made self-propelled rods can be described by the model of the circle swimmer. An example of this would be vibrated polar granular particles [6], macroscopic rods or colloidal particles [12, 14]. Additionally, even pedestrians, wearing blindfolds and ear-plugs, perform similar motions in vast areas without any obstacles [15].

In most studies of active particles the self-propulsion of the particles points along a specified orientation. However, the internal motor that drives the particles' motion

does in general not exactly coincide with the orientation axis of the particle. In this case, the slight offset leads to an effective internal torque that causes deviations from straight-line motion. We consider an internal motor responsible for the self-propulsion and the torque the particle experiences without discussing the complex mechanisms inside this motor.

Summary

In this Bachelor thesis results are presented of studies of the dynamics of a single Brownian circle swimmer in confining potentials using both a theoretical treatment and computer simulations. In the first chapter we introduce the Brownian circle swimmer and explain the model describing its dynamics in two dimensions under the influence of different external potentials. Before describing motions confined by external potentials, we briefly discuss the analytic solution and simulation results of motion in the bulk situation, i.e. in the absence of these potentials, as a reference for the confined cases. In chapter 2 simulations of different configurations for circular and ring-shaped potentials are presented and discussed. In chapter 3 we focus on the so-called steady state configuration. In order to gain a better understanding of this configuration, we analyze it by theoretical means and simulations. Finally, we summarize the main points of this thesis, provide a short outlook of problems that are still to be solved, and suggest further extensions of the model of a Brownian circle swimmer.

1 The Model of a Brownian Circle Swimmer

1.1 Definition of the Model

We first introduce the model, defining what is meant by a Brownian circle swimmer. In two dimensions, we model it as a rod-like colloidal particle of length L and width d. The vector $\mathbf{r} = (x, y)$ gives the position of the particle's center of mass and the unit vector $\hat{\mathbf{u}} = (\cos\phi, \sin\phi)$ represents its orientation with ϕ defined as the angle between the rod's orientation and the x-axis.

A characteristic of the circle swimmer is that a systematic force $\mathbf{F} = \mathcal{F}\hat{\mathbf{u}}$ acts along its orientation and a systematic torque $\mathbf{T} = \mathcal{T}\hat{\mathbf{e}}_z$ acts perpendicular to the (x, y)-plane the particle moves in. Because of these simple applied forces, the swimmer performs circular trajectories which explains its name. Figure 1.1 illustrates the circle swimmer and the characterizing parameters.

It is assumed that the swimmer is a particle of mesoscopic length-scale ranging from some nanometers to micrometers and that it is surrounded by a solvent. The solvent interacts with the particle in two ways that are in particular damping the swimmers' movement and perturbing its trajectory as an effect of temperature.

In this model we consider a very viscous solvent so that motions are overdamped, i.e. we assume that the momenta relax instantaneously. At finite temperature the circular movement is perturbed, displaying Brownian-type motion which results from numerous collisions of the swimmer with the solvent particles. Since the frequency of these collisions is extremely large ($\sim 10^{21}$ per second) there is no need to analyze every single collision. To describe the effect of these collisions, we simply use the well-known statistical considerations that have been used to model random Brownian motion. [5, 16]

In order to gain a better understanding of certain processes, we also examine the model at – as we call it – 'zero temperature', meaning that we neglect the random fluctuations caused by collisions between the swimmer and the jostling solvent particles.

1.2 Equations of Motion

We model the overdamped Brownian dynamics of the self-propelled particle by the following two Langevin equations [16] of motion, using dots to denote time derivatives:

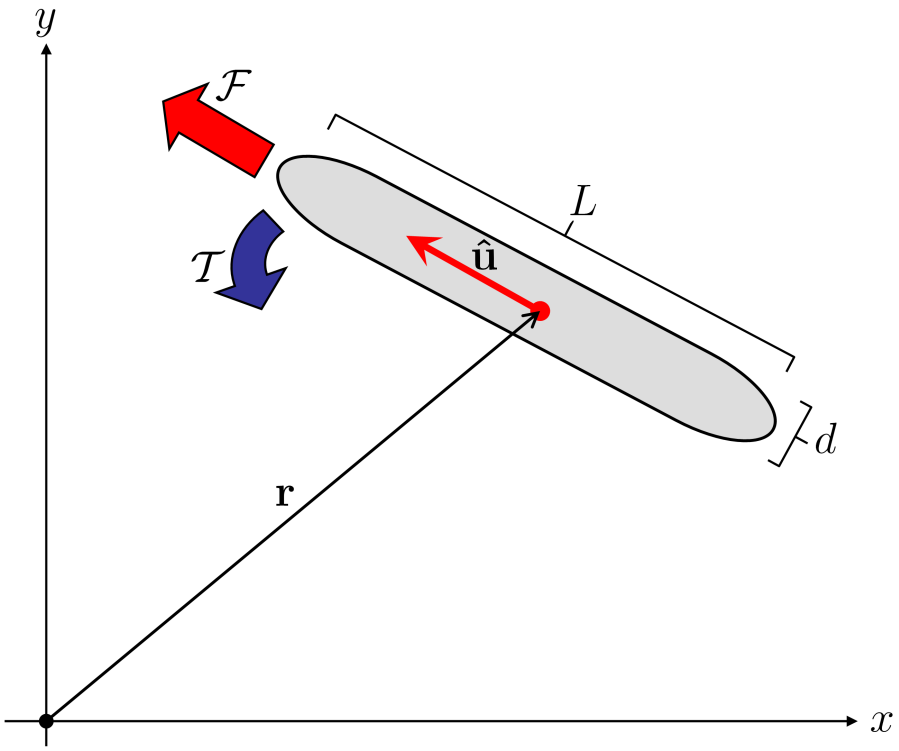

Figure 1.1: Diagram of a Brownian circle swimmer. The broad red arrow indicates the self-propulsive force $\mathcal{F}$ and the blue one the internal torque $\mathcal{T}$.

$$\dot{\mathbf{r}} = \beta \mathbf{D}(\mathbf{F} - \vec{\nabla} V(\mathbf{r}, \phi) + \mathbf{f}), \tag{1.1}$$

$$\dot{\phi} = \beta D_r(\mathcal{T} - \partial_\phi V(\mathbf{r}, \phi) + \tau). \tag{1.2}$$

In the latter equation the short-time diffusion constant in rotational direction is denoted by D_r. In the former equation, however, in order to describe the diffusive behavior in a proper way, we have to define the short-time diffusion tensor $\mathbf{D}$. This is due to the fact that the circle swimmer is not isotropic and the diffusion in every spatial direction is dependent on the swimmer's orientation $\hat{\mathbf{u}}$. The short-time diffusion tensor

$$\mathbf{D} = D_\parallel(\hat{\mathbf{u}} \otimes \hat{\mathbf{u}}) + D_\perp(\mathbb{1} - \hat{\mathbf{u}} \otimes \hat{\mathbf{u}})$$

is given in terms of the short-time diffusion constants along its orientation $D_\parallel$ and perpendicular to its orientation $D_\perp$. In this thesis $\beta = (k_B T)^{-1}$ is the inverse thermal energy, $\mathbb{1}$ the unit tensor and $\otimes$ the dyadic product. The term $V(\mathbf{r}, \phi)$ denotes an external potential that is confining the Brownian circle swimmer and is applied in chapter 2.

In the Langevin picture, Brownian motion is incorporated via stochastic uncorrelated forces $\mathbf{f}$ and torques τ that cause random trajectories of the particles. We then may separate the force $\mathbf{f}$ into two independent components that are parallel ($f_\parallel$)

and perpendicular ($f_\perp$) to the rod's orientation $\hat{\mathbf{u}}$. We assume the random quantities $f_\parallel, f_\perp, \tau$ to be characterized as Gaussian white noise given by the properties

$$\langle f_\parallel \rangle = \langle f_\perp \rangle = \langle \tau \rangle = 0, \tag{1.3}$$

$$\langle f_\parallel(t_1) f_\parallel(t_2) \rangle = \frac{2}{\beta^2 D_\parallel} \delta(t_1 - t_2), \tag{1.4}$$

$$\langle f_\perp(t_1) f_\perp(t_2) \rangle = \frac{2}{\beta^2 D_\perp} \delta(t_1 - t_2), \tag{1.5}$$

$$\langle \tau(t_1) \tau(t_2) \rangle = \frac{2}{\beta^2 D_r} \delta(t_1 - t_2). \tag{1.6}$$

Here $\langle A \rangle$ denotes the noise average of the quantity A. Equation (1.3) reveals that there is no preferred direction of the random forces. Further, equations (1.4), (1.5) and (1.6) describe the variance of the particular random quantities and suggest that the forces and torques are not correlated in time. The prefactors of the delta distribution $\delta(t)$ are the outcome of the *fluctuation dissipation theorem* [16].

For simplicity, we denote all lengths in units of L, energies in units of β^{-1} and times in units of $\tau_B = L^2/D_\parallel$. Following these conventions, we can explore different scenarios by simply changing the dimensionless quantities $\beta\mathcal{T}$ and $\beta\mathcal{F}L$. Additionally, we introduce the assumption that the swimmer is a long and thin rod, i.e. $L \gg d$, and therefore the diffusion constants are assumed to be inter-related [3]:

$$D_\parallel = \tfrac{2}{3} D_r L^2,$$
$$D_\perp = \tfrac{1}{2} D_\parallel.$$

The most simple scenario one can think of is at zero temperature without confinement. We call this case the 'deterministic swimmer' as without temperature effects equations (1.1) and (1.2) provide a non-stochastic solution that we briefly discuss. Applying this scenario the equations of motion reduce to $\dot{\mathbf{r}} = D_\parallel \beta\mathcal{F}\hat{\mathbf{u}}$ and $\dot{\phi} = D_r \beta\mathcal{T}$. By simply integrating we obtain the solution:

$$\mathbf{r} = R_{\text{det}} \left[\sin(\omega_0 t) \hat{\mathbf{e}}_x + (1 - \cos(\omega_0 t)) \, \hat{\mathbf{e}}_y \right] \quad \text{with} \quad R_{\text{det}} = \frac{D_\parallel \mathcal{F}}{D_r \mathcal{T}}. \tag{1.7}$$

The trajectory of the deterministic swimmer is a perfect circle with the radius R_{det} which depends on the ratio of the internal properties of the rod. The circular frequency ω_0 of the particle equals the spinning frequency $\dot{\phi}$. Therefore, we obtain

$$\omega_0 = \dot{\phi} = D_r \beta\mathcal{T}. \tag{1.8}$$

Figure 1.2 illustrates the trajectory of the deterministic swimmer.

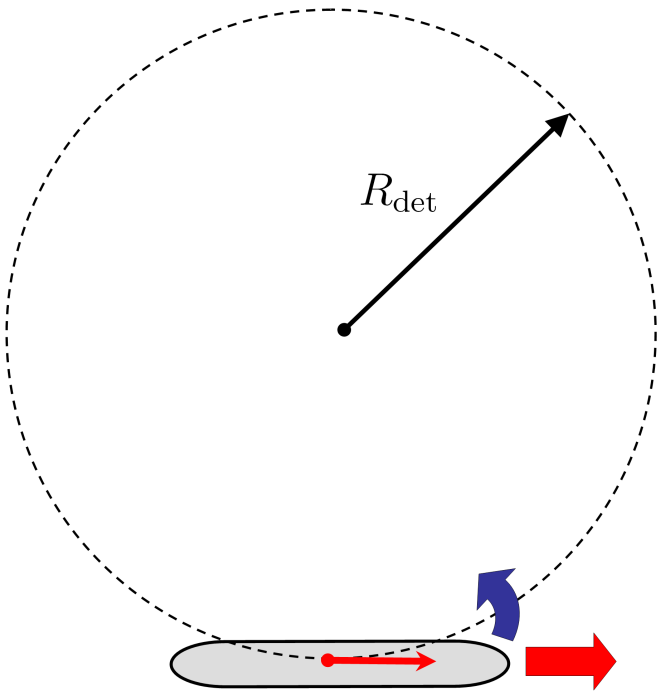

Figure 1.2: Movement of the Brownian circle swimmer in the absence of temperature effects and confining potentials. The trajectory is a circle with the radius $R_{\text{det}} = D_{\parallel}\mathcal{F}/(D_r\mathcal{T})$.

1.3 Free Brownian Circle Swimmer

Before we introduce the confining potential, it is beneficial to study, as a reference scenario, the dynamics of a Brownian Circle Swimmer at finite temperature in the absence of any potential or obstacles. For obvious reasons, we refer to a swimmer in this setting as the 'free circle swimmer'. The dynamics of a free circle swimmer have already been discussed yielding exact analytical expressions for the first moment $\langle \mathbf{r}(t) - \mathbf{r}_0 \rangle$ at finite temperature [18]. Also, this solution has been compared to computer simulation confirming the calculations. Therefore, just the results are presented and briefly discussed.

We start to analyze this scenario by observing a sample realization of a random trajectory of the free circle swimmer that is presented in figure 1.3. Note, that the circular movement of the swimmer is apparent in this figure, but because of the random Langevin terms in the equations of motion, the circles described by the trajectory are not perfect. The circular motion is perturbed by small fluctuations.

To arrive at more general conclusions concerning the random trajectory of the circle swimmer, it is reasonable to examine the average trajectory over many realizations of these randomly generated trajectories. Thankfully, in the case of the free circle swimmer, this mean trajectory may be determined analytically.

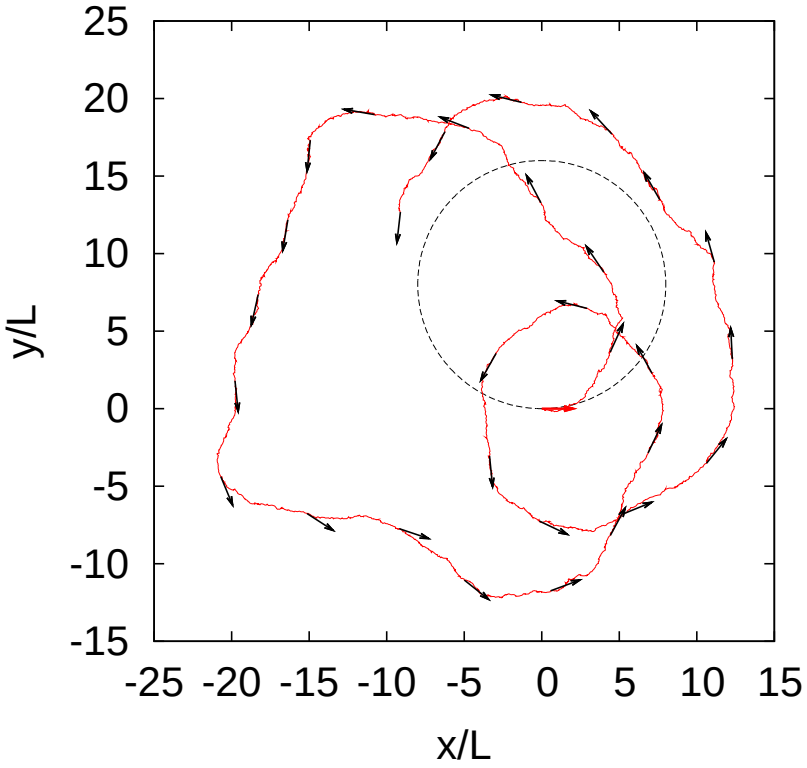

Figure 1.3: Typical realization of the free circle swimmer for $\beta\mathcal{F}L = 60$, $\beta\mathcal{T} = 5$ and $t_{\max} = 2\,\tau_B$. The deterministic trajectory is displayed by the dashed black circle with the radius $R_{\text{det}} = 8\,L$.

Generally, it is possible to calculate all moments of the free circle swimmer's orientation ϕ and position $\mathbf{r}$. For the purpose of this Bachelor thesis, however, we focus on the first moments of $\mathbf{r}$ and ϕ since we compare the averaged trajectories to the confined cases in chapter 2 and point out deviations. The first moments are given by

$$\langle \phi(t) - \phi_0 \rangle = \omega_0 t, \tag{1.9}$$

$$\langle \mathbf{r}(t) - \mathbf{r_0} \rangle = \lambda \left[D_r \hat{\mathbf{u}}_0 - \omega_0 \hat{\mathbf{u}}_0^{\perp} - e^{-D_r t} \left(D_r \langle \hat{\mathbf{u}} \rangle + \omega_0 \langle \hat{\mathbf{u}}^{\perp} \rangle \right) \right], \tag{1.10}$$

using the following abbreviations:

$$\lambda = \frac{\beta D_{\parallel} \mathcal{F}}{D_r^2 + \omega_0^2},$$

$$\begin{aligned} \hat{\mathbf{u}}_0 &= (\cos\phi_0, \sin\phi_0), & \hat{\mathbf{u}}_0^{\perp} &= (-\sin\phi_0, \cos\phi_0), \\ \langle \hat{\mathbf{u}} \rangle &= (\cos\langle\phi\rangle, \sin\langle\phi\rangle), & \langle \hat{\mathbf{u}}^{\perp} \rangle &= (-\sin\langle\phi\rangle, \cos\langle\phi\rangle). \end{aligned}$$

Here, $\mathbf{r}_0$ denotes the initial position, ϕ_0 the initial orientation of the circle swimmer and ω_0 the circular frequency we defined in the deterministic scenario. The averaged trajectories at different internal properties $\mathcal{F}$ and $\mathcal{T}$ are shown in figure 1.4. In case $\mathcal{F}L \gg \mathcal{T}$ the swimmer moves on average rather straight in the

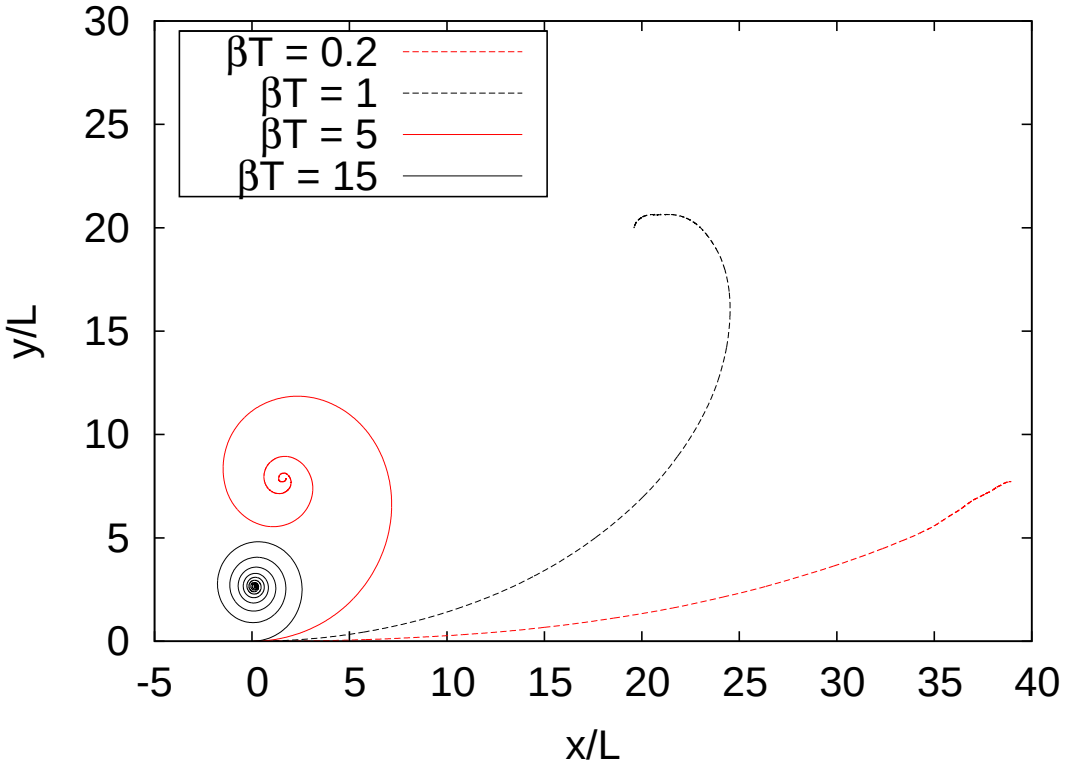

Figure 1.4: Averaged trajectories $\langle \mathbf{r}(t) - \mathbf{r}_0 \rangle$ of the simulations of a free circle swimmer [18]. The parameter $\beta \mathcal{F} L = 60$ is fixed and different values $\beta \mathcal{T} = 0.2, 1, 5, 15$ are applied. In every scenario the swimmer starts at $\mathbf{r}_0 = 0$ and its orientation points along the x-axis ($\phi_0 = 0$). The duration of the simulation is $t_{\max} = 5\,\tau_B$.

direction of the initial orientation with a slight tendency to the direction the torque acts to. In the case of stronger internal torques the mean trajectory describes a *spira mirabilis* and converges in the middle of the spiral. The stronger the torque, the more circulations are performed before the average trajectory converges.

2 Confining Potentials

In this chapter we introduce different external repulsive potentials and discuss their influence on the dynamics of the Brownian circle swimmer. After determining the properties of the surface of a potential wall, we construct different confinements. We probe potentials that can be separated into two classes, i.e. circular and ring-shaped ones. In each class of potential we focus on different parameters and examine their influence on the dynamic behavior of the circle swimmer. However, hydrodynamic interactions between the wall and the circle swimmer which lead in general to an additional diffusion tensor [7] are not taken into account in this model.

The potentials we consider are of radial symmetry so it is reasonable to make use of an appropriate coordinate system. In this case the use of polar coordinates yields the most simple access to discuss the dynamics of the confined swimmer. We introduce the variables $r = |\mathbf{r}|$ and Θ as the angle between $\mathbf{r}$ and the x-axis to give the position of the rod's center of mass. To describe the swimmer's orientation we define ϑ as the angle $\hat{\mathbf{u}}$ makes with $\mathbf{r}$. Note, that we can express ϑ easily in terms of the other two angles by $\vartheta = \phi - \Theta$ and that ϑ describes the swimmers orientation towards the potential wall. Figure 2.1 gives an overview of the variables that we introduced.

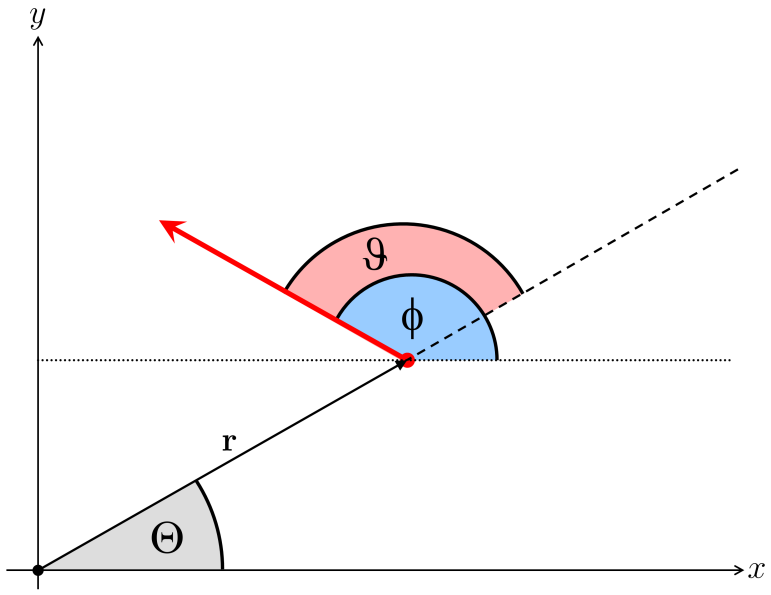

Figure 2.1: The polar coordinates that are used in the description of a swimmer in confinement of radial symmetry are shown.

2.1 Definition of the External Potential

Now that we have defined the properties of the internal mechanisms responsible for the movement of a Brownian circle swimmer, we may characterize how it interacts with an external confining potential. In this thesis soft potentials are mainly used in simulations, whereas in theoretical considerations we will usually, for simplicity, refer to the case of hard potential walls. The repulsive behavior of the confining wall in respect of a single colloidal sphere is described by the Lennard-Jones-Potential:

$$v(\mathbf{r}) = \beta^{-1} \left(\frac{L}{R - r} \right)^n . \tag{2.1}$$

The exponent n is a measure of how hard the potential wall is. A greater value for n means a stronger repulsion but a shorter interaction length. Starting from equation (2.1) we derive the interaction effects a rod-like particle experiences from a potential of circular symmetry.

We therefore consider a set of N colloidal particles that are firmly connected along a line of length L and the distance between each colloid is $\Delta l = L/N$, such as it is shown in figure 2.2. This set of colloids can be described by the two variables $\mathbf{r}$ and ϑ, denoting the center of mass of this set and its orientation.

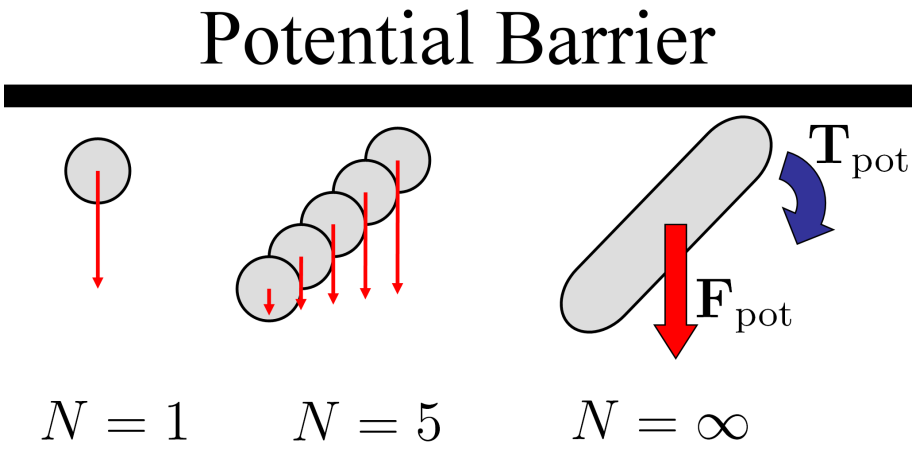

Figure 2.2: Derivation of the interaction of a rod-like swimmer with the potential wall. *Left*: Repulsion of a single colloidal particle. *Middle*: Repulsion acting on every segment of a set of five colloidal particles. Since the repulsion on every segment is different there will be an effective torque $\mathbf{T}_{\text{pot}}$ and an effective force $\mathbf{F}_{\text{pot}}$ acting on the whole set. *Right*: In the limit of infinitely many segments the rod-like particle is described. The effective force $\mathbf{F}_{\text{pot}}$ and torque $\mathbf{T}_{\text{pot}}$ are shown.

$$V_N(\mathbf{r},\vartheta) = \frac{1}{N}\sum_{k=0}^{N-1} v\left(\mathbf{r} + (k - \tfrac{N-1}{2})\Delta l\,\hat{\mathbf{u}}\right) \tag{2.2}$$

$$= \frac{1}{\beta N}\sum_{k=0}^{N-1}\left(\frac{L}{R - \sqrt{r^2 + \Delta l^2 + 2r\Delta l\cos\vartheta}}\right)^n \tag{2.3}$$

Now letting $N \to \infty$ at fixed length L, the sum of the interactions of the individual colloids making up the rod becomes an integral:

$$V(\mathbf{r},\vartheta) = (\beta L)^{-1}\int_{-\frac{L}{2}}^{\frac{L}{2}}\left(\frac{L}{R - \sqrt{r^2 + l^2 + 2rl\cos\vartheta}}\right)^n \mathrm{d}l. \tag{2.4}$$

Since solving the integral from equation (2.4) leads to a very complex expression, a good approximation is needed to simplify the problem. A sensible approximation is the assumption that locally seen the potential wall is planar instead of curved. This approximation is valid for the case that the length of the rod L is much smaller than the radius R of the potential. Using this approximation we obtain

$$\begin{aligned}\tilde{V}(\mathbf{r},\vartheta) &= (\beta L)^{-1}\int_{-\frac{L}{2}}^{\frac{L}{2}}\left(\frac{L}{R - r + l\cos\vartheta}\right)^n \mathrm{d}l \\ &= -\frac{L^{n-1}}{\beta(n-1)\cos\vartheta}\left(\frac{1}{(R - r + \frac{L}{2}\cos\vartheta)^{n-1}} - \frac{1}{(R - r - \frac{L}{2}\cos\vartheta)^{n-1}}\right).\end{aligned} \tag{2.5}$$

With equation (2.5) we are able to calculate the force $\mathbf{F}_{\mathrm{pot}} = F_{\mathrm{pot}}\,\hat{\mathbf{e}}_r$ and torque $\mathbf{T}_{\mathrm{pot}} = T_{\mathrm{pot}}\,\hat{\mathbf{e}}_z$ on the swimmer by the potential wall by simply taking partial derivates of the potential $\tilde{V}(\mathbf{r},\vartheta)$ with respect to r and ϑ. These terms are given explicitly as:

$$F_{\mathrm{pot}} = -\frac{L^{n-1}}{\beta\cos\vartheta}\left(\frac{1}{(R - r + \frac{L}{2}\cos\vartheta)^n} - \frac{1}{(R - r - \frac{L}{2}\cos\vartheta)^n}\right), \tag{2.6}$$

$$T_{\mathrm{pot}} = \tan\vartheta\left[\tilde{V}(\mathbf{r},\vartheta) - \frac{L^n}{2\beta}\left(\frac{1}{(R - r + \frac{L}{2}\cos\vartheta)^n} + \frac{1}{(R - r - \frac{L}{2}\cos\vartheta)^n}\right)\right]. \tag{2.7}$$

In figure 2.3 the force F_{pot} and the torque T_{pot} resulting from the potential are displayed in dependence on different configurations (r,ϑ) of the swimmer to gain a better understanding of equations (2.6) and (2.7). The left diagram in figure 2.3 shows the dependence of the force F_{pot} on the radial distance r from the origin of

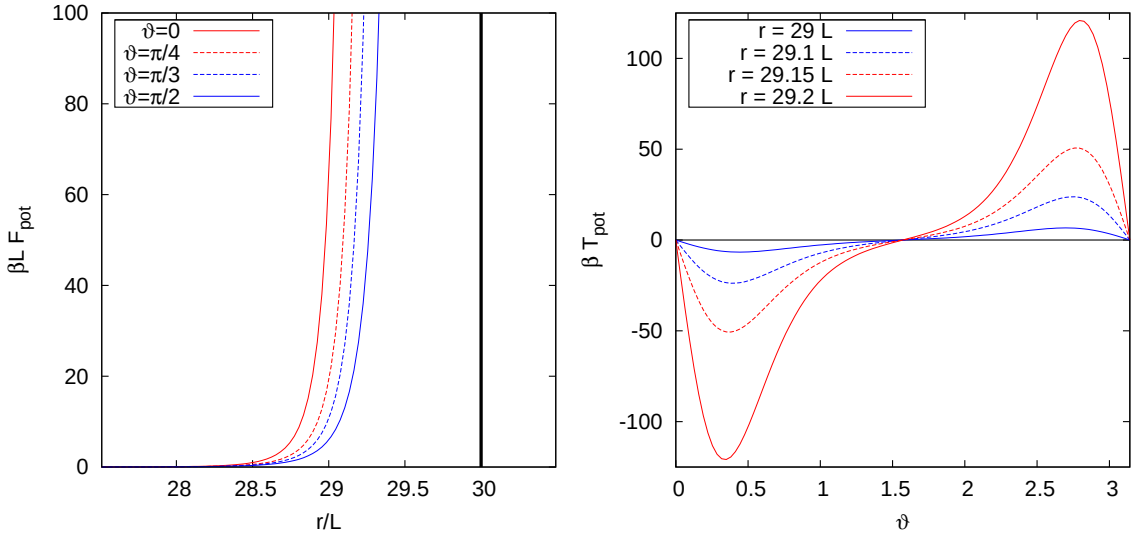

Figure 2.3: *Left:* Repulsive force F_{pot} resulting from the potential in dependence on radial distance of the swimmer's center of mass. The potential barrier is located at $R = 30\,L$ and pictured by the black line. Different curves represent different configurations of the angle ϑ. *Right:* Torque T_{pot} resulting from the potential in dependence on the angle ϑ of the particle. The different curves indicate different radial distances from the origin to the circle swimmers' position. The potential barrier is located at $R = 30\,L$.

the potential. The potential wall is located at a radial distance $R = 30\,L$ and it is marked by the black line. The different curves represent configurations at different angles the swimmer makes with the barrier. One can easily see that the solid red curve at $\vartheta = 0$ is the most adverse configuration for the swimmer as for every distance the repulsion is the strongest. In addition, if the rod is parallel to the wall, i.e. $\vartheta = \pi/2$ represented by the solid blue curve, this case provides the least repulsion at every distance.

The right diagram in figure 2.3 shows the dependence of the torque T_{pot} on the angle ϑ. The different lines represent different distances r from the origin and the potential wall is located at $R = 30\,L$. There are two configurations at which T_{pot} equals zero. The first is at $\vartheta = 0$, i.e. the swimmer is perpendicular to the wall, and the other at $\vartheta = \pi/2$ when the swimmer is located parallel to the wall. The former configuration is a very unstable one since small fluctuations in ϑ lead to a strong torque rotating the rod away from the perpendicular orientation. In the case of the latter situation the rod is far more stable as every fluctuation in ϑ results in a torque directed opposite to the direction of that fluctuation. Note, that even at small variations in the swimmer's position r the external torque T_{pot} differs strongly.

2.2 Dynamics in the Circular Potential

In this section we discuss the behavior of a single Brownian circle swimmer in a circular confinement. The potential itself can be described by just one parameter, the radius of the confining circle, R. First, we observe a sample realization of the circle swimmer in confinement to gain insight into the behavior in confinement. Then, we explore the effects of different sizes of the confinement by varying the radius R at a fixed ratio of the internal properties $\zeta = \mathcal{T}/(\mathcal{F}L)$. We also examine the effects of different values of ζ at a fixed size of the confinement.

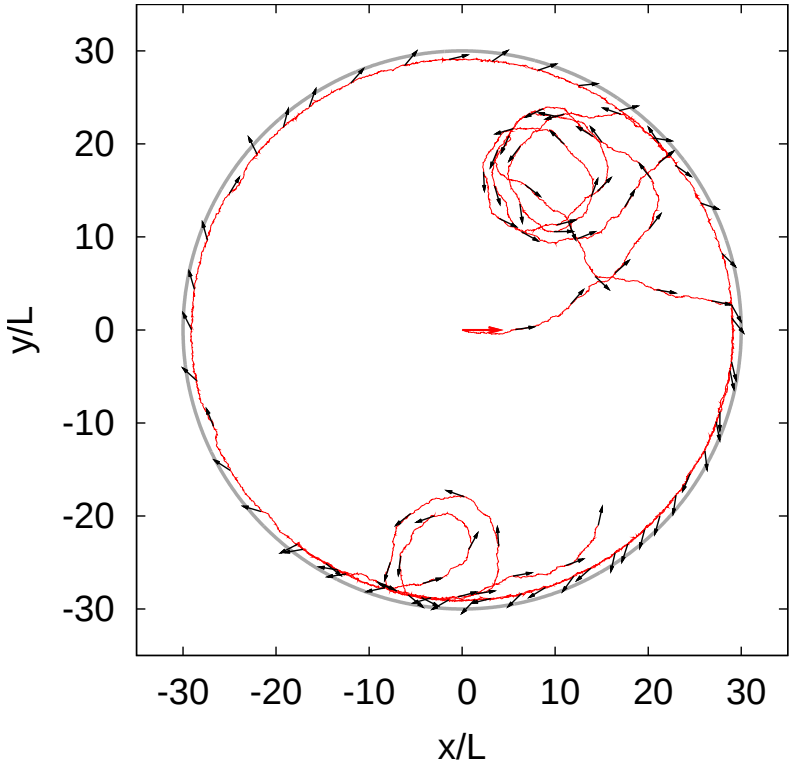

Figure 2.4: Typical trajectory of a Brownian circle swimmer in circular confinement with the radius $R = 30\,L$ at $\beta\mathcal{F}L = 60$, $\beta\mathcal{T} = 5$ and $t_{\max} = 10\,\tau_B$. The swimmer starts in the middle of the potential ($r_0 = 0$) pointing along the x-axis ($\phi_0 = 0$).

In order to focus on a few important parameters and to examine their impact on the dynamics of a circle swimmer, we apply the following values to the other parameters in each simulation: The exponent n of the Lennard-Jones potential indicating the hardness of the confining wall is chosen to be $n = 6$. The duration of each realization is chosen to be $t_{\max} = 10\,\tau_B$ at discrete time-steps $\Delta t = 10^{-5}\,\tau_B$. A simulation usually consists of $N_s = 10\,000$ single and independent realizations allowing good averaging over the randomly generated trajectories. As an initial condition every particle starts at the same configuration ($\mathbf{r}_0 = 0, \phi_0 = 0$), i.e. the swimmer is located in the middle of the confinement and its orientation points

along the x-axis. In all figures the trajectory is given by the red curve, the initial configuration is indicated by the red vector and the instantaneous orientation at some points is displayed by black vectors.

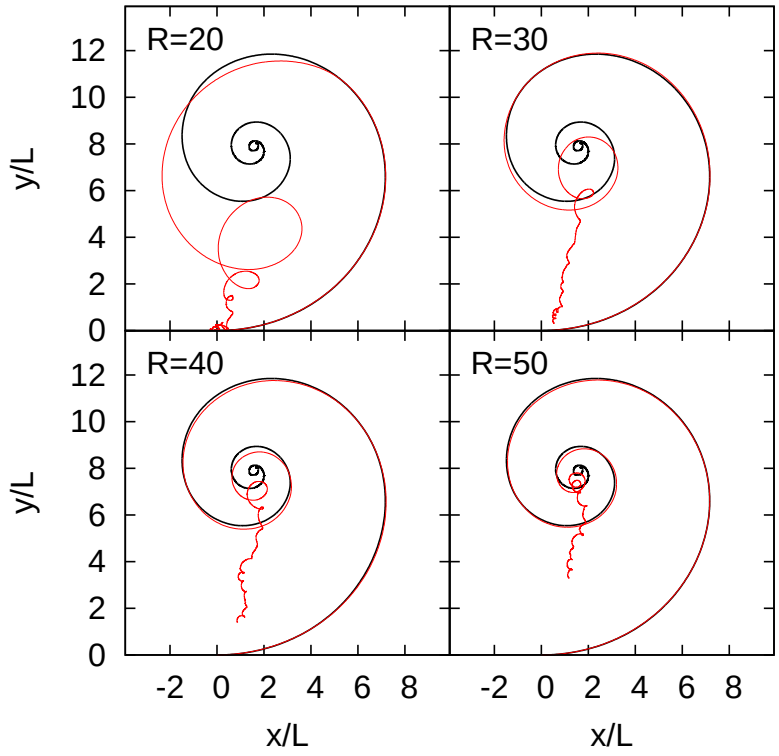

Figure 2.5: The first moments $\langle \mathbf{r}(t) - \mathbf{r}_0 \rangle$ of the free circle swimmer and a circle swimmer in circular confinement with different radii $R/L = 20, 30, 40, 50$ at $\beta \mathcal{F} L = 60$, $\beta \mathcal{T} = 5$ and $t_{\max} = 10\,\tau_B$.

First, let us consider a single random trajectory such as it is shown in figure 2.4. By analyzing this sample trajectory, we notice that the swimmer performs some random circular movement at the beginning. Near the potential wall the swimmer adopts a special sliding mode that guides it along the potential barrier. This interesting property of interaction with the confinement will be examined in a more detailed way in chapter 3 and we will refer to the configuration the swimmer adopts as the 'steady state' (r_s, ϑ_s).

Next, we compare the confined case to the free swimmer. Therefore we choose the same internal force $\beta L \mathcal{F} = 60$ and torque $\beta \mathcal{T} = 5$ that we had used in the simulation of the free swimmer. The only parameter changed in the different simulations is the radius R of the confining circular potential. Results of the averaged trajectories are shown in figure 2.5.

In these figures, the average trajectory of the rod at the beginning of the simulation is quite similar to that of the free circle swimmer, at which its motion describes a spira mirabilis. But instead of converging to the middle of this spiral, the average trajectory of the confined swimmer deviates more and more from that of the

free swimmer. Finally, the first moment tends back to the middle of the circular potential.

The effect of using larger radii R is that deviations from the shape of a spira mirabilis develops at later times than for the cases of confining potentials with small radii. This is to be expected as the swimmer experiences the confinement for larger radii at later times since it has to move larger distances by diffusion to arrive from the initial position at the potential wall.

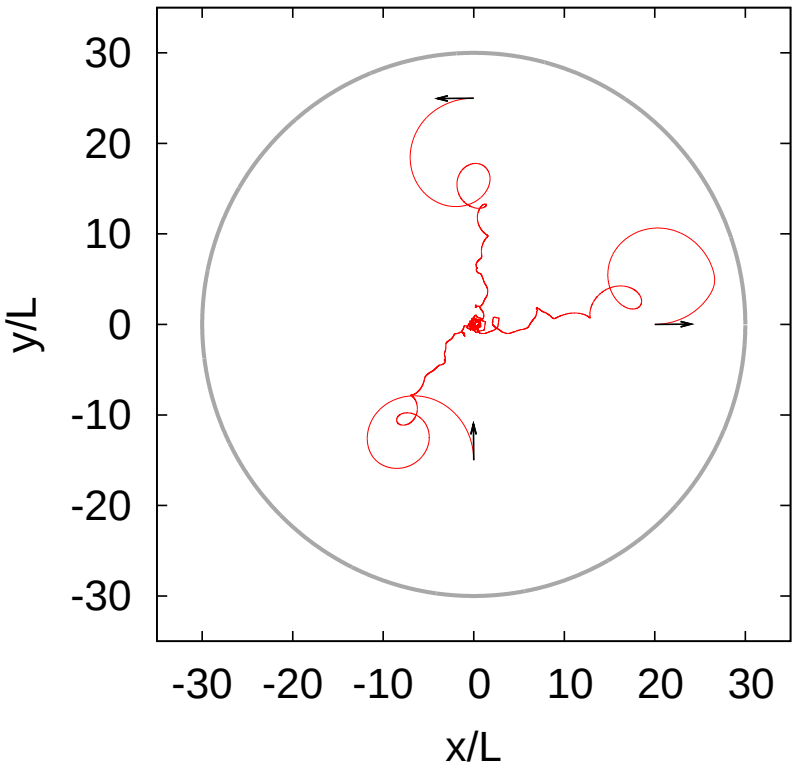

Figure 2.6: Averaged trajectories $\langle \mathbf{r}(t) - \mathbf{r}_0 \rangle$ of the Brownian circle swimmer in circular confinement ($R = 30\ L$) with different initial configurations (r_0, ϕ_0) given by the black vectors. The internal properties $\beta \mathcal{F} L = 60$, $\beta \mathcal{T} = 5$ are fixed and the duration of each simulation is $t_{\max} = 20\, \tau_B$.

In figure 2.6 we increase the duration of the simulations by a factor of 5 compared to our initial ones to examine the long-time behavior of the system using different initial configurations (r_0, ϕ_0). We confirm our expectations that independent from the initial configuration the mean trajectory of the circle swimmer converges to the middle of the potential.

However, the circle swimmer itself is in most cases not located in the middle of the potential as one can see in figure 2.7 where the particle density ρ in radial direction at the end of the simulation is shown for different values of $\beta \mathcal{T}$. The blue line represents the density distribution for the internal parameters used in figures 2.5 and 2.6. We notice that near the potential wall at $r \approx 30\, L$ there is a maximum in the density profile. This means that in most cases the swimmer is located near

the potential wall and not in the middle of the confinement. Therefore we conclude that after a certain time the circle swimmer is uniformly distributed in the angle Θ so its average position is zero.

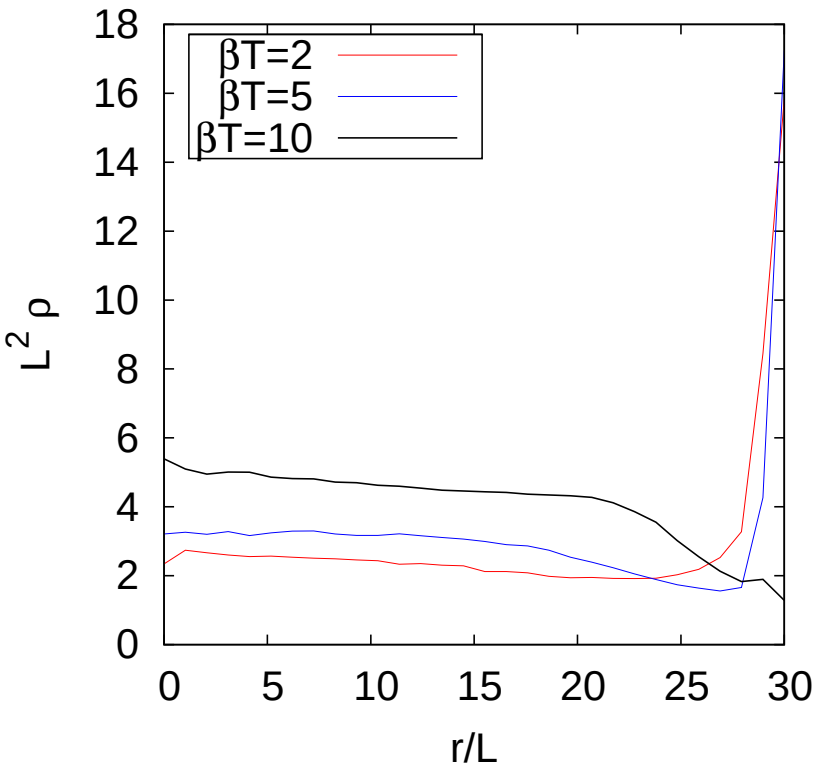

Figure 2.7: The different particle densities ρ in radial direction at $t = 10\,\tau_B$ and fixed $\beta\mathcal{F}L = 60$ in dependence on different torques $\beta\mathcal{T}$ in circular confinement with the radius $R = 30\,L$.

In radial direction the particle density ρ is constant except near the potential wall. In the cases $\beta\mathcal{T} = 2$ and $\beta\mathcal{T} = 5$ the density ρ increases whereas it decreases at greater torques such as in the case $\beta\mathcal{T} = 10$. This observation can be explained due to the formation of a stable or semi-stable steady state configuration (r_s, ϑ_s) the swimmer adopts near the potential wall for small torques. At larger torques the configuration (r_s, ϑ_s) becomes unstable.

In order to better understand the behavior of the swimmer near the potential barrier, we measure the angle ϑ of the circle swimmer whenever it is located near the confinement, i.e. $29\,L \leq r \leq 30\,L$. The histogram shown in figure 2.8 displays how often during the $N_s = 10\,000$ single realizations a particle with the corresponding angle ϑ was located near the confinement.

We notice that there are two maxima, one of a positive value ϑ_+ and the other of a negative value ϑ_-. This means that the circle swimmer strongly prefers certain configurations $(r, \vartheta_\pm)$ near the potential wall. In the cases $\beta\mathcal{T} = 2$ and $\beta\mathcal{T} = 5$ the number of particles at ϑ_- is much larger than at ϑ_+. From this fact we can conclude that the configuration (r, ϑ_-) at which the rod points to clockwise direction is more

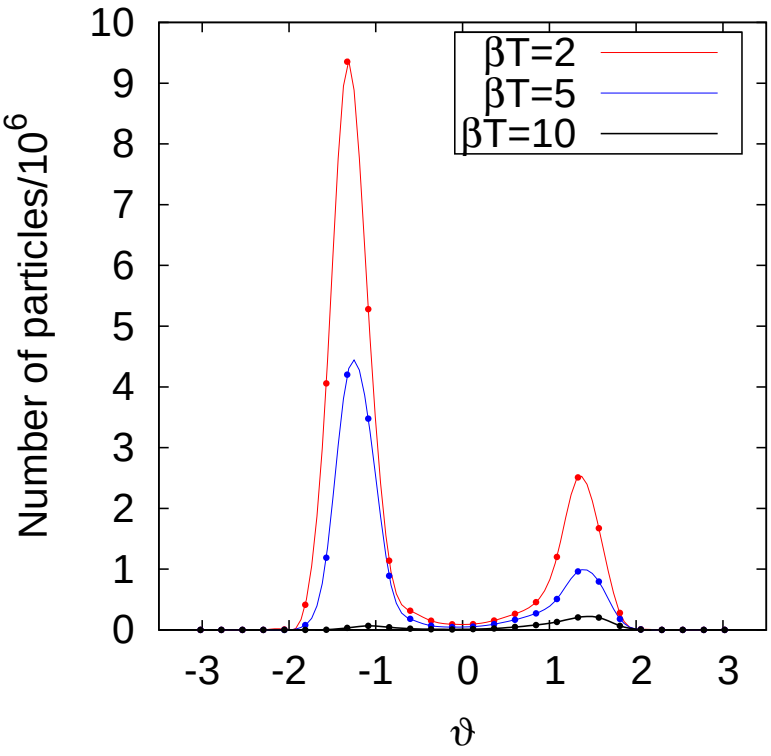

Figure 2.8: Number of particles that were detected near the potential wall ($29\,L \leq r \leq 30\,L$) in dependence on ϑ . The internal force $\beta L\mathcal{F} = 60$ is applied and the different curves indicate different values of $\mathcal{T}$. The dots represent the results of the measurement. To improve clarity the points of data are connected by cubic splines.

stable. Obviously, this is the steady state configuration (r_s, ϑ_s) we observed before. The maximum at ϑ_+ can be explained by two matter of facts. First, we only take particles into account that are located close to the confinement. In our discussion of the external potential in section 2.1 and figure 2.3 we noticed that the least repulsion F_{pot} is given at $\vartheta = \pm\pi/2$ so it is more likely for these particles to come close to the potential wall. In addition, we recognized that at $\vartheta = \pm\pi/2$ the circle swimmer is in the most stable configuration concerning the torque T_{pot} that results from the potential. Due to these two influences we observe a maximum at ϑ_+ although this is no sliding mode.

In the case $\beta\mathcal{T} = 10$ hardly any particle is located near the potential wall which confirms the low particle density we noticed in figure 2.7. Moreover, the maximum at ϑ_+ is greater than at ϑ_- in contrast to the cases we discussed before. Obviously this means that no sliding mode is avaiable in this setting.

2.3 Dynamics in the Ring-Shaped Potential

We next apply a ring-shaped potential. In principle, the ring-shaped potential is the superposition of two concentric repulsive circular potentials with different radii $R_s < R_l$. The swimmer is confined in a channel of width $D = R_l - R_s$ which is asymmetric due to the different values of the radii since the curvature of the inner potential is greater than the curvature at the outer potential. First, we make ourselves familiar with a sample trajectory of a circle swimmer in ring-shaped confinement. We then explore the impact of different ratios of the internal properties $\zeta = \mathcal{T}/(\mathcal{F}L)$ while constant radii R_s, R_l are applied.

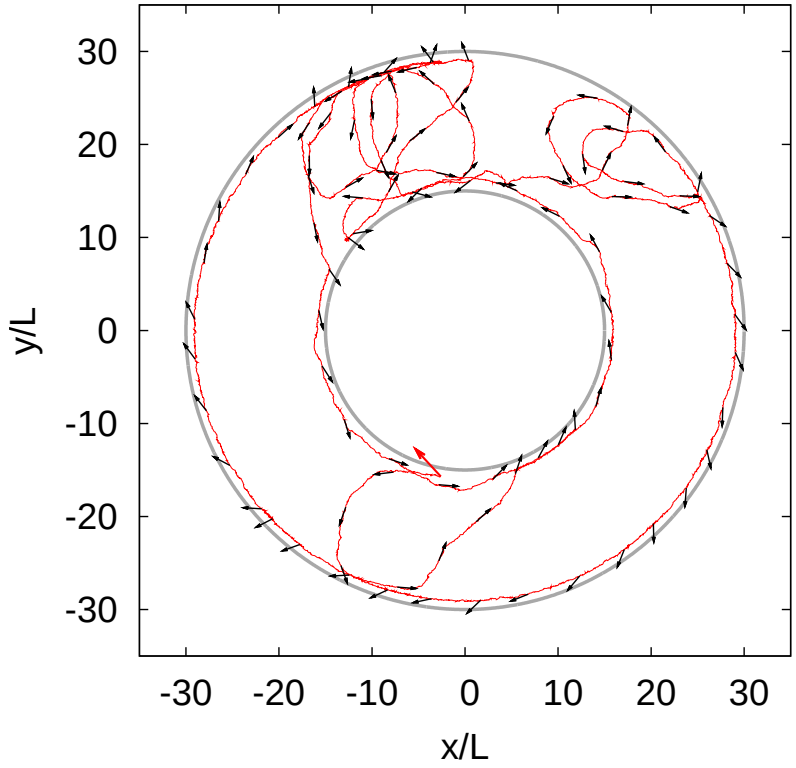

Figure 2.9: Sample realization of the trajectory of a Brownian circle swimmer in ring-shaped confinement with $R_l = 30\,L$ and $R_s = 15\,L$ at $\beta\mathcal{F}L = 60$, $\beta\mathcal{T} = 5$ and $t_{\max} = 10\,\tau_B$.

In simulations using the ring-shaped potential we especially focus on the steady state results. Comparing the first moments of the swimmer in ring-shaped confinement with the mean trajectory in circular confinement is complicated by the fact that we can no longer start with an initial configuration of the swimmer being at in the middle of the potentials, since this position is not accessible in the ring-shaped confinement. The task, therefore, is to observe the swimmer's dynamics independently of its initial state $(\mathbf{r}_0, \phi_0)$. For this reason, we sample trajectories of the swimmer with different initial configurations in each simulation. The initial state parameters r_0 and ϕ_0 are chosen to be uniformly distributed. As we can

not expect that the distribution of the swimmer at early points in its trajectory is the same for the initial states, we only consider statistics of the trajectory after long times $t \geq 10\,\tau_B$, expecting that the circle swimmer is finally independent of its initial conditions. For this reason, the duration of each simulation is increased to $t_{\max} = 20\,\tau_B$ with time-steps $\Delta t = 10^{-5}\,\tau_B$. As with the circular confinement, we apply soft potentials ($n = 6$). The data presented in the figures are obtained by averaging over $N_s = 10\,000$ independent realizations.

A typical trajectory of the swimmer in the ring-shaped potential is shown in figure 2.9. In this sample trajectory with $\beta L\mathcal{F} = 60$ and $\beta\mathcal{T} = 5$ we observe two different steady state configurations, one at each potential wall. In case the swimmer is in the steady state at the outer potential it moves in clockwise direction whereas at the inner potential it moves in counter-clockwise direction. The question whether both steady states are equal in stability is raised and further analyzed in chapter 3.

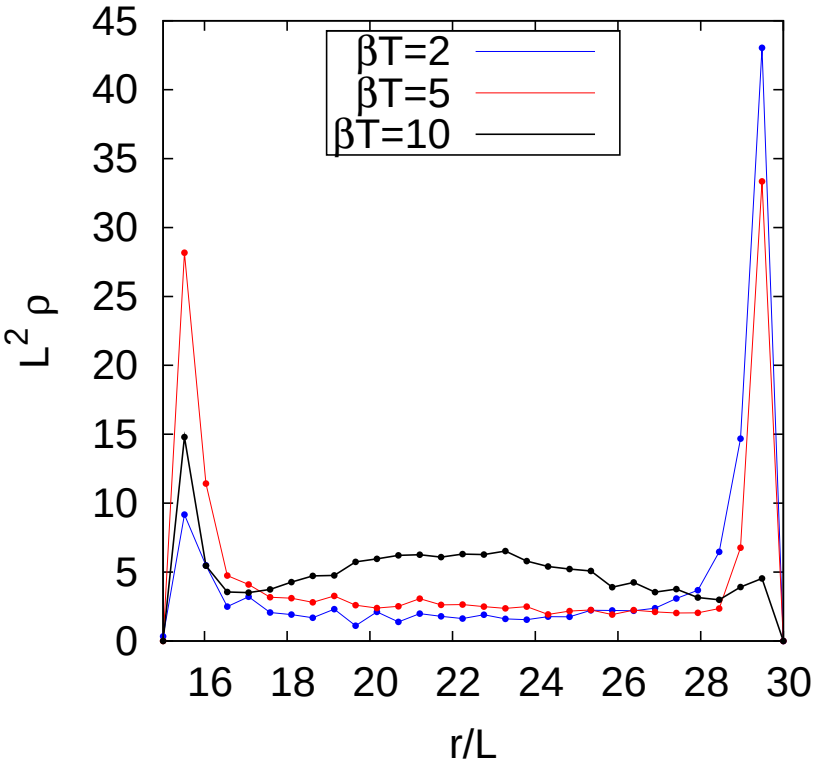

Figure 2.10: Particle densities in radial direction at fixed $\beta\mathcal{F}L = 60$ and different $\beta\mathcal{T} = 2, 5, 10$ at the time $t = 10\,\tau_B$. The inner radius is $R_s = 15\,L$ and the outer radius is $R_l = 30\,L$. Dots denote the measured results.

We examine the impact of different internal torques $\mathcal{T}$ on the steady state configurations in ring-shaped confinement. Therefore we measure the particle density ρ in radial direction applying various internal torques as shown in figure 2.10. The densities give an idea of how stable steady state configurations are. Clearly, for a small $\mathcal{T}$ we can find a stable steady state configuration only at the outer potential which is indicated by the maximum at $r \approx 30\,L$. At the inner potential the density

is nearly as low as in the middle of the channel. By applying greater torques the density at the inner potential grows which means that a sliding mode at the inner wall appears, whereas the steady state at the outer wall becomes more and more unstable. As with circular confinement, applying greater internal ratios $\zeta = \mathcal{T}/(\mathcal{F}L)$ results in the disappearance of the steady state configuration at the outer potential wall but still we can find a small maximum in the density profile at the inner wall.

The reason why there is no stable steady state configuration at low values for ζ at the inner potential is due to the fact that the deterministic radius $R_{\text{det}} \sim \zeta^{-1}$ we introduced in chapter 1 is larger than the radius of the inner circle R_s of the ring-shaped confinement. As we show in the theoretical considerations in the next chapter the condition $R_{\text{det}} \leq R_s$ has to be fulfilled to allow a steady state configuration. The different stabilities at the walls at greater ζ is an effect of the asymmetry of the channel. In the limit as $R_s, R_l \to \infty$ but at constant width D the confinement becomes a symmetric channel at which the observed effect disappears.

3 The Sliding Mode

By analyzing the trajectory of a swimmer in confining potentials, we observe that there is a special configuration at which the swimmer slides along the potential barrier and we refer to it as the sliding mode or steady state configuration. The fact that the probability of finding the swimmer near the potential walls is much higher than elsewhere gives an idea that this sliding mode is stable or at least semi-stable. This sliding mode has already been observed and discussed in a symmetric channel [18]. Here, the diffusion of the Brownian circle swimmer in the channel is strongly enhanced under appropriate conditions.

In this chapter we analyze the sliding mode in circular and ring-shaped confinement more exactly. For this reason we at first try to understand this steady state configuration (r_s, ϑ_s) by theoretical considerations. Then, we compare the obtained results to numerical simulations in the absence of fluctuations and finally to simulation data at finite temperature. We also end with some general conclusions, confirmed by simulations.

A particle near the potential barrier is repulsed by the external force F_{pot} and experiences a torque T_{pot} caused by the repulsive potential. Assume, the swimmer is in a configuration at which the internal force $\mathcal{F}$ moves the particle back to the potential wall and the internal torque $\mathcal{T}$ turns it towards the confinement. Then, there might be an equilibrium of forces and torques so that effectively the swimmer stays at a certain distance r_s and adopts a special angle ϑ_s in respect of the wall.

Nevertheless, the swimmer is not motionless in the configuration (r_s, ϑ_s) since it propagates along the potential wall with the steady state velocity $\mathbf{v}_s = v_s \hat{\mathbf{e}}_\Theta$. The aim of the theoretical considerations is be find out the dependence of the steady state angle ϑ_s on the relation of the two internal quantities $\zeta = \mathcal{T}/(\mathcal{F}L)$.

3.1 Theoretical Deduction

As mentioned in the introductory part of this chapter the circle swimmer still moves along the potential barrier but it does not change its configuration (r_s, ϑ_s). We will take this characteristic into account by formulating the equations of motion in the absense of fluctuations as follows:

$$\dot{\mathbf{r}} \cdot \hat{\mathbf{e}}_r = \beta \mathbf{D}(\mathbf{F} - \vec{\nabla} V(\mathbf{r}, \vartheta)) \cdot \hat{\mathbf{e}}_r = 0, \tag{3.1}$$

$$\dot{\phi} = \beta D_r(\mathcal{T} - \partial_\vartheta V(\mathbf{r}, \vartheta)) = \Omega_0. \tag{3.2}$$

In this notation we make use of the unit vector in r-direction $\hat{\mathbf{e}}_r = (\cos\Theta, \sin\Theta)$. Further, we define the lap frequency Ω_0 as the average amount of rounds the particle moves along the circular potential in steady state configuration (r_s, ϑ_s) in a time interval. In the case of zero temperature the lap frequency is given by $\Omega_0 = \dot{\Theta}$. Equation (3.1) can easily be understood by the fact that the radial distance r_s is constant so there will be no change in r-direction. Therefore $\dot{\mathbf{r}}$ is perpendicular to the unit vector $\hat{\mathbf{e}}_r$, i.e. the scalar product of both vectors equals zero.

Equation (3.2) is justified because in steady state the swimmer stays at a constant angle ϑ_s towards the potential wall but ϕ denotes the angle towards the x-axis in cartesian coordinates. As we are discussing potentials of circular symmetry the orientation vector $\hat{\mathbf{u}}$ will rotate steadily while the swimmer moves along the confinement. After performing one round along the potential the swimmer will have turned around exactly one time and the expression $\dot{\phi} = \Omega_0$ is true.

The steady state velocity $\mathbf{v}_s = v_s\hat{\mathbf{e}}_\Theta$ is parallel to the potential wall. The lap frequency Ω_0 at steady state is constant because the absolute value of the steady state velocity v_s does not change in time. Both quantities are related and given by:

$$v_s = \beta \sin\vartheta_s \left(D_\parallel \mathcal{F} + (D_\parallel - D_\perp) F_{\text{pot}}\right) \hat{\mathbf{e}}_\Theta, \tag{3.3}$$

$$\Omega_0 = \frac{v_s}{r_s}. \tag{3.4}$$

Using both, equation (3.1) and (3.2), we obtain a system of equations that can only be solved numerically. To simplify this system of equations and give a qualitative analytical solution we consider the limit of hard walls as an approximation, i.e. $n \to \infty$. In this limit only the behavior of the front tip of the rod is of importance. The analytical solution is given by:

$$r = (R - \tfrac{L}{2}\cos\vartheta_s), \tag{3.5}$$

$$\cos^2\vartheta_s = \frac{2\sin\vartheta_s L - 3r\zeta}{3r(\zeta - 1)}. \tag{3.6}$$

In figure 3.1 the theoretical results of the simplified equations are plotted. On the x-axis ζ is displayed and on the y-axis the cosine of ϑ. The color of the curves indicates different radii of a circular potential.

We notice that for a given value of ζ up to four solutions of the equation (3.6) exist. Two solutions are at negative and two at positive values of $\cos\vartheta$. Essentially, this means that we can distinguish two different cases. In the first case the swimmer is confined by the potential and the swimmer slides along the barrier in clockwise direction at $\cos\vartheta \leq 0$. In the other case, the swimmer is located outside of the potential moving in counter-clockwise direction at $\cos\vartheta \geq 0$. Obviously, in the case of the ring-shaped confinement the steady state configuration the swimmer adopts at the outer potential is in general not symmetric to the configurations the swimmer adopts at the inner potential. In the limit as $R_s, R_l \to \infty$ but at constant width D

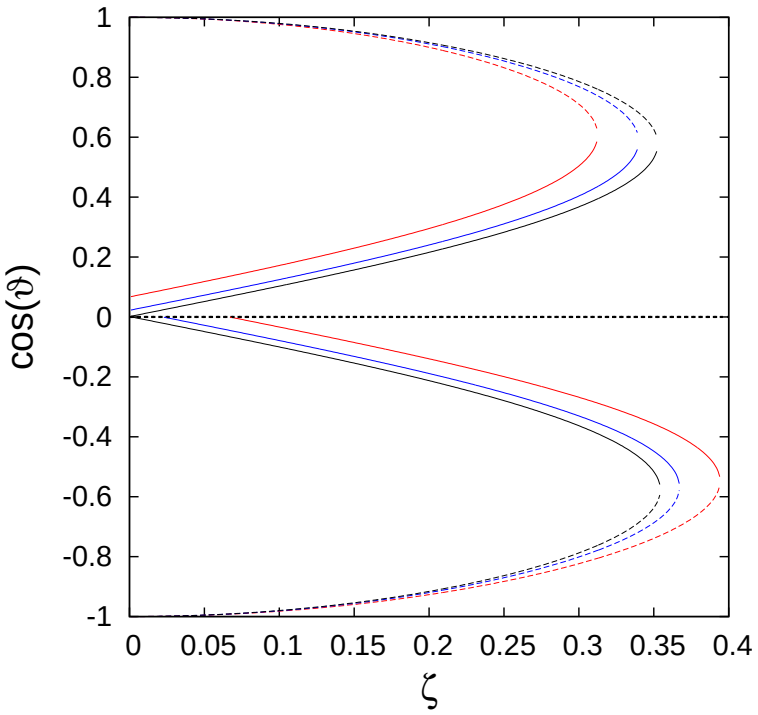

Figure 3.1: Theoretical predictions of $\cos(\vartheta_s)$ in steady state configuration in dependence on the ratio $\zeta = \mathcal{T}/(L\mathcal{F})$. The dashed curves symbolize instable solutions that are not expected to be observed in simulations. The different colored curves are the solutions in a confinement with the radius $R_1 = 10\,L$ (red), $R_2 = 30\,L$ (blue) and $R_3 = 500\,L$ (black).

we get a symmetric channel. This expectation is confirmed by the black curve in figure 3.1 that represents $\cos\vartheta_s$ in a large potential with $R_3 = 500\,L$ which is, for our purpose, close to infinity. In this case the solutions are symmetric.

Additionally, in each of these cases the swimmer can adopt two configurations of different stability. The dashed curves in figure 3.1 represent the unstable solution of the steady state. This configuration already collapses at small fluctuations in the angle ϑ. The other solution, marked by straight lines in figure 3.1, remains resistant against small variations in ϑ.

Another interesting conclusion is that above a certain threshold ζ_{th} no solutions can be found anymore. This threshold depends on the radius of the external potential and on the location of the swimmer whether it is inside or outside of the confinement.

In figure 3.2 the theoretical predictions are compared to the simulations at zero temperature. We notice discrepancies between theory and simulation depending on the hardness of the potential wall n. This can be explained by the fact that we used the limit of hard walls ($n \to \infty$) as an approximation in the theory. We notice that the theory provides a good description only for hard walls.

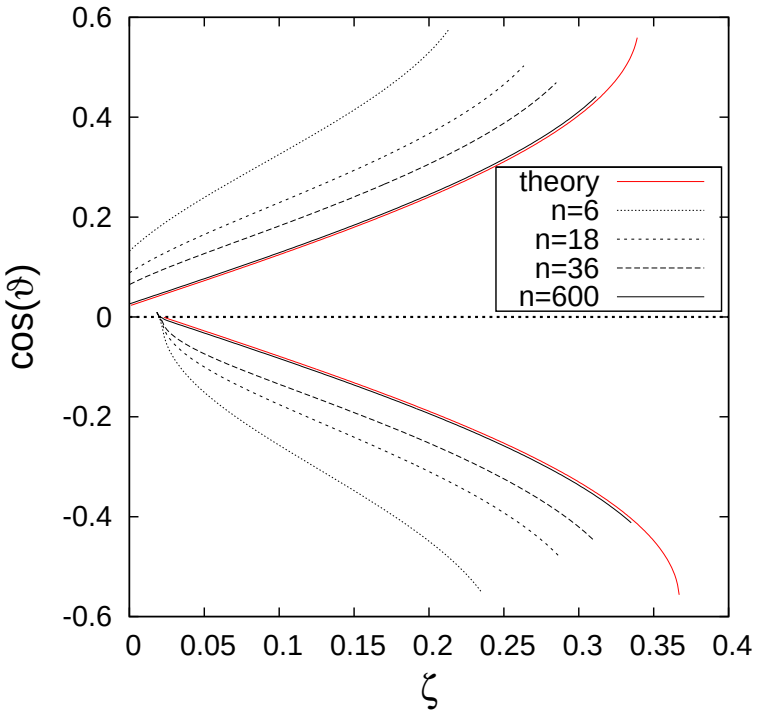

Figure 3.2: The theoretical results (red) and the simulation results (black) are displayed. The different dashed black curves indicate different values of the exponent n of the Lennard-Jones potential used in the simulation. Only the stable solutions are shown as there are no instable modes observed in simulations. In the simulations a circular potential with the radius $R = 30\,L$ has been applied.

One more difference between theory and simulation can be observed near the threshold ζ_{th} at which no steady state is possible anymore. In the curves obtained from simulations the steady state seems to collapse at some $\zeta < \zeta_{\text{th}}$ depending on the hardness of the potential wall n. The effect responsible for this fact is not completely understood and it is not clear whether this is due to the approximation in theory or some noise from simulations.

3.2 Mobility of the Circle Swimmer

So far, we have analyzed the behavior of a Brownian circle swimmer in the steady state configuration at zero temperature and different hardness of the confining walls. The question we are now heading for is in which way the internal properties of the swimmer and the external potentials influence the mobility of the particle in clockwise or counter-clockwise direction at finite temperatures.

We will discuss this question by using long-time simulations at which the lap

frequency $\Omega = \langle \dot{\Theta} \rangle$ is evaluated. Negative values of Ω mean that the particle moves in clockwise direction. Since the propagating velocity v depends on the self-propulsive force $\mathcal{F}$ we keep the quantity $\beta \mathcal{F} L = 60$ fixed for all simulations. Otherwise, the mean velocity at steady state would also be changed which would complicate the interpretation of the results. The parameter ζ is varied by altering the internal torque $\mathcal{T}$.

In order to achieve good statistical results, we increase the duration of the simulations drastically to $t_{\max} = 1\,000\,\tau_B$. Due to this increase of simulation time we apply larger time-steps $\Delta t = 10^{-4}\,\tau_B$ and we decrease the number of realizations to $N = 5\,000$. The quantity Ω is estimated by averaging over the N realizations for each given ζ. Every simulation starts at the same initial configuration (r_0, ϑ_0) but since the duration of every single realization is increased by a factor of 100 the impact of the initial state is negligible.

Note, that the obtained values for Ω are influenced by some effects of the set-up of the simulations. The lap frequency Ω is dependend on the distance r of the circle swimmer from the middle of the confinement. Whenever the rod is close to the origin of the potential, $\dot{\Theta}$ becomes very large and therefore the lap frequency Ω also increases. In the case of the ring-shaped potential the steady state configuration at the inner potential wall is of a greater angular velocity $\dot{\Theta}$ than the configuration at the outer wall because the sliding mode at the inner potential is closer to the origin of the confinement. In the following interpretation of the simulation data we should keep these effects in mind to allow qualitative conclusions of the dynamical behavior.

To understand the basic processes in this simulation it is beneficial to discuss at first the behavior at zero temperature as a reference scenario. Here, the deterministic swimmer is supposed to be confined by a circular potential and the lap frequency is given by Ω_0. In the absence of an internal torque, $\mathcal{T} = 0$, this case provides the maximum lap frequency Ω_0 that can be achieved in clockwise direction since the swimmer is located parallel to the wall, i.e. $\vartheta = \pm\pi/2$. By increasing the internal torque Ω_0 decreases because the quantity $\cos(\vartheta)$ increases at larger values of ζ as shown in figure 3.3, meaning that ϑ becomes more acute. At a certain ratio ζ_{th}, Ω_0 becomes abruptly zero. This is the threshold at which deterministically no steady state is possible anymore and therefore the swimmer does not slide along the potential wall so the lap frequency Ω_0 collapses.

Beside the lap frequency there is another mean angular velocity $\xi = \langle \dot{\phi} \rangle$ we observe and we will refer to as the spinning frequency. The dashed curves indicate the angular velocity ξ the particle spins with. In the case of small internal torques the spinning frequency of the deterministic swimmer ξ_0 is identical with the lap frequency Ω_0. Whenever the particle performs a round in the confinement it exactly rotates one time as we already assumed in the theoretical deduction in the beginning of this chapter. Beyond the threshold ζ_{th} at which the steady state collapses ξ_0 becomes abruptly positive, i.e. the swimmer spins in counter-clockwise direction and increases linearly with the torque (see figure 3.4). This behavior can be understood, since no steady state is available. So the deterministic swimmer's

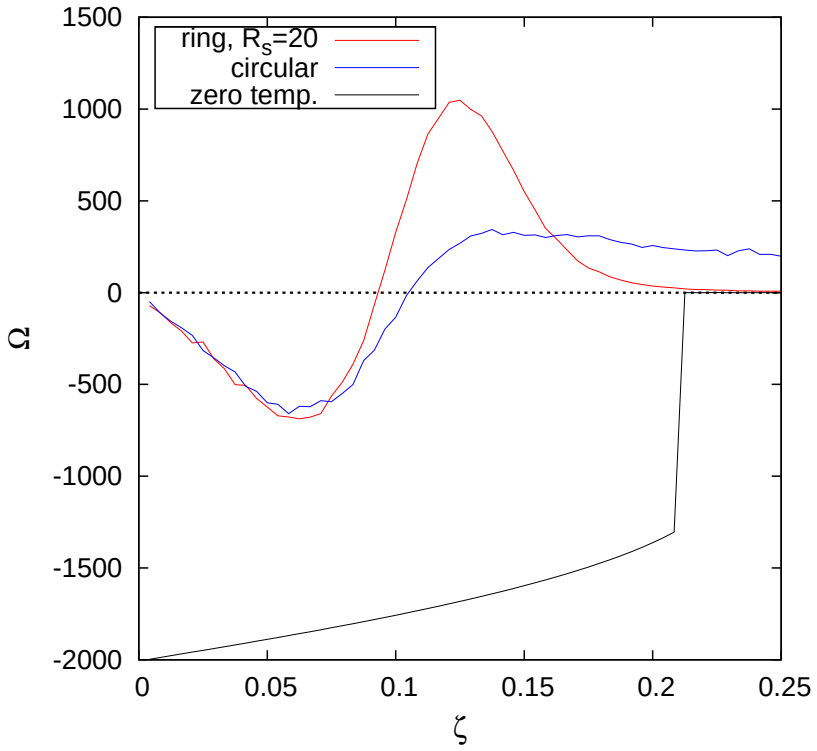

Figure 3.3: The lap frequencies Ω are shown in dependence on ζ. The black curve is the lap frequency Ω_0 of the deterministic swimmer and the colored ones are the lap frequencies of the confined cases. The applied duration of each simulation is $t_{\max} = 1\,000\,\tau_B$ with the time-steps $\Delta t = 10^{-4}\,\tau_B$.

trajectory is a perfect circle with the spinning frequency $\xi_0 = \omega_0 = \beta D_r \mathcal{T}$ according to equation (1.8). The relation $\xi_0 \sim \mathcal{T}$ explains the linear increase of ξ_0 with ζ.

Now, after studying the deterministic case, we turn to the simulations in different potentials at finite temperature. Comparing the simulations at $\zeta \approx 0$ to the deterministic case we notice that at finite temperatures the lap frequency Ω is nearly zero but increases with ζ in clockwise direction. At a certain ratio ζ_l, which is smaller than ζ_{th}, we notice a maximum of the lap frequency Ω in clockwise direction. Another maximum of Ω in the counter-clockwise direction appears at ζ_s. Note, that ζ_s is larger than ζ_l but it is still smaller than the deterministic threshold ζ_{th}. This second maximum depends on the shape of the confinement since it is much more pronounced in the ring-shaped potential. For $\zeta > \zeta_s$ the lap frequency Ω decays to zero in different manners, depending on the potential. In the circular potential the decay is much slower, whereas in the ring-shaped case Ω decays rather fast.

Focusing on the spinning frequency ξ we observe contrary to the deterministic case $\xi > \Omega$ for any value of ζ. At $\zeta > \zeta_{\text{th}}$ the spinning frequency from the simulations ξ is asymptotic to the deterministic spinning frequency ξ_0. Here, the circle swimmer performs small circles but does not move along the potential wall.

The behavior of the swimmer at finite temperature varies from the behavior

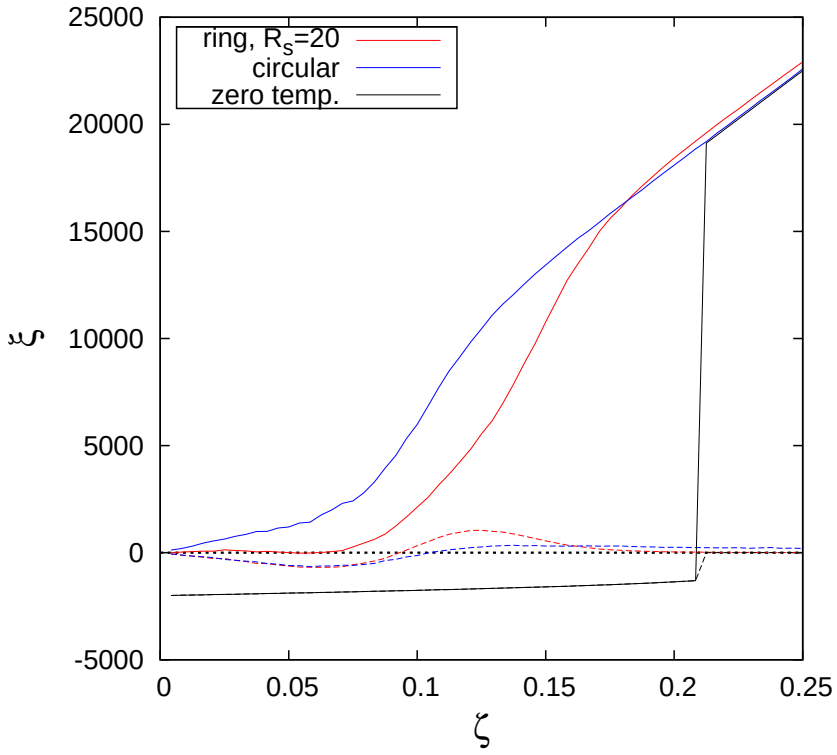

Figure 3.4: The spinning frequencies ξ are shown in dependence on ζ. As reference the lap frequencies Ω are also displayed as dashed curves. The applied duration of each simulation is $t_{\max} = 1\,000\,\tau_B$ with the time-steps $\Delta t = 10^{-4}\,\tau_B$.

discussed in the absence of temperature effects. The deviations allow conclusions about the dynamics at finite temperature. In the absence of an internal torque one can explain the different behavior at zero and at finite temperature by the fact that random fluctuations especially in the angle provide a certain probability to at first leave the steady state and then adopt a sliding configuration moving in the opposite direction. Since there is no internal torque the steady state is of the same stability in both, counter-clockwise and clockwise, directions. In principle, at low torques $\mathcal{T}$, i.e. if $R_{\text{det}} > R$, there is also a sliding mode in both directions but due to the preferred rotation caused by the internal torque the sliding mode in counter-clockwise direction is of lower stability. This conclusion is confirmed by the increasing lap frequency Ω in clockwise direction.

For larger ζ up to ζ_l where we can find the maximum of the lap frequency Ω in clockwise direction the stability of the steady state increases since the probability that the particle leaves the wall by fluctuations against the direction of the torque is reduced. The fact that ξ does not coincide with Ω means that the probability to leave the steady state still is greater than zero. The following decrease of stability can be explained by another effect that occurs. From the theoretical considerations and the evaluation of simulations we know that for $\zeta > \zeta_{\text{th}}$ the steady state collapses.

If fluctuations in the angle act in the direction of the torque it is enhanced, whereas fluctuations against the internal force diminish the effective propulsion. The combination of these fluctuations might result in an effective ratio $\zeta = \mathcal{T}/(\mathcal{F}L)$ that is greater than ζ_{th} so the steady state collapses. At a larger systematic torque $\mathcal{T}$ even at smaller fluctuations this flip process occurs. Similar conclusions were reached by a discussion of the circle swimmer in a symmetric channel [18]. Here, the flipping rate, i.e. the swimmer's probability of leaving the steady state, is estimated by means of non-Hamiltonian rate theory in dependence on ζ.

As an effect of the asymmetry of the channel in the ring-shaped case the swimmer adopts a stable steady state configuration at the inner potential wall when the steady state at the outer potential becomes less stable. This conclusion is confirmed by the fact that the lap frequency Ω becomes positive which means that the particle moves in counter-clockwise direction. At even greater torques Ω decreases to zero. This means that there is no stable sliding configuration and the rod will not move in one preferred direction. In the circular confinement we also observe a positive maximum at ζ_s of Ω which decays very slowly for greater ζ. This is an effect of the simulation set-up as we discussed before. The swimmer performs small circles with an average radius R_{det}. Most of the time $\dot{\Theta} \approx 0$ but whenever the swimmer diffuses in the middle of the potential, i.e. the performed circle overlaps with the origin of the potential, $\dot{\Theta}$ increases significantly. Since $R_{\text{det}} \sim \zeta^{-1}$ the performed circles become smaller with greater ζ so the probability of overlapping decreases which is responsible for the slow decay of Ω in case of the circular potential.

The general conclusion from this simulation is that at a certain ratio $\zeta = \mathcal{T}/\mathcal{F}L$ the steady state is most stable in respect of fluctuations and the mobility Ω of a Brownian circle swimmer is at maximum in a certain direction. Further, in an asymmetric channel there are different values ζ_l and ζ_s at which the mobility is at maximum in different directions.

Conclusion

Finally, after the discussion of different confinements and the steady state we sum up and outline the essential insights. In the absence of confining potentials the first moment of the so called free circle swimmer converges by describing a spira mirabilis. Compared to the bulk case, in circular confinement the first moment of the Brownian circle swimmer behaves in a similar way for short times. As an influence of the external potential the long time behavior of the mean trajectory deviates from the one of the free circle swimmer. The averaged trajectory converges to the center of the potential meaning that the probability distribution of the swimmer is uniformly distributed in the angle. In radial direction the swimmer is in the case of $\zeta < \zeta_{\text{th}}$ often located near the potential wall due to the steady state configuration.

In ring-shaped potentials different steady states are possible. This configurations are dependent on the the ratio $\zeta = \mathcal{T}/(\mathcal{F}L)$ and on the radius R of the confinement. In principle, beyond a certain threshold ζ_{th} the steady state configuration becomes instable and the probability of finding the swimmer near the potential wall decreases fast.

The steady state configuration is calculated theoretically for the limit of hard walls and simulated for walls of different hardness. We notice that there is still a discrepancy between simulations at soft walls and theoretical predictions that are not negligible. In long-time simulations we obtain a qualitative understanding of the mobility of of the Brownian circle swimmer in clockwise and counter-clockwise direction. At a certain relation between the internal quantities $\mathcal{T}$ and $\mathcal{F}L$ the swimmer, disturbed by Brownian motion, exploits the steady state configuration of greatest stability to achieve a maximum of mobility.

Outlook

In this Bachelor thesis some basic characteristics of the Brownian circle swimmer are considered and examined. As the analysis of self-propelling particles in general and of the Brownian circle swimmer in particular is a recent object of research there is still a number of effects to study further. Due to the limited range that is provided for the Bachelor thesis some aspects of interest could not be taken into account further. The following suggestions are a sketch of interesting problem that can be studied further.

A more quantitative analysis of the stability of the steady state by means of rate theory would give a more detailed understanding of the dynamical effects. This thesis just focused on potentials of radial symmetry. Of course, discussing other

potentials may reveal other effects and stable configurations. Further, the potential walls can be designed differently by using, for example, hard walls. In the ring-shaped confinement the influence on the dynamic behavior by using different exponents n_1, n_2 for the inner and outer Lennard-Jones potential might provide some different effects. Moreover, one can investigate whether the potential can be manipulated in a way that the swimmer will find its stable configuration at one wall and avoid the opposite one to even improve the mobility in that direction.

Besides variation in the settings, describing the dynamics of the Brownian circle swimmer in the Smoluchowski picture will give an alternative view on this problem focusing on the time evolution of particle densitiy.

An obvious extension is a model of many Brownian circle swimmers interacting via hard-body or even hydrodynamic interactions which would yield new effects on the dynamics.

Bibliography

[1] Berg, H. C., and Turner, L. Chemotaxis of bacteria in glass-capillary arrays. *Biophys. J. 58* (1990), 919.

[2] Dhar, P., Fischer, T. M., Wang, Y., Mallouk, T. E., Paxton, W. F., and Sen, A. Autonomously moving nanorods at a viscous interface. *Nano Lett. 6* (2006), 66.

[3] Dhont, J. K. G. *An Introduction to Dynamics of Colloids*. Elsevier, Amsterdam, 1996.

[4] DiLuzio, W. R., Turner, L., Mayer, M., Garstecki, P., Weibel, D. B., Berg, H. C., and Whitesides, G. M. Escherichia coli swim on the right-hand side. *Nature 435* (2005), 1271.

[5] Doi, M., and Edwards, S. F. *The Theory of Polymer Dynamics*. Clarendon Press, Oxford, 1986.

[6] Dreyfus, R., Baudry, J., Roper, M. L., Fermigier, M., Stone, H. A., and Bibette, J. Microscopic artificial swimmers. *Nature 437* (2005), 862.

[7] Dufresne, E. R., Squires, T. M., Brenner, M. P., and Grier, D. G. Hydrodynamic coupling of two Brownian spheres to a planar surface. *Phys. Rev. Lett. 85* (2000), 3317.

[8] Friedrich, B., and Jülicher, F. Chemotaxis of sperm cells. *PNAS 104* (2007), 13256.

[9] Helbing, D. Traffic and related self-driven many-particle systems. *Rev. Mod. Phys. 73* (2001), 1067.

[10] Helbing, D., Johansson, A., and Al-Abideen, H. Dynamics of crowd disasters: An empirical study. *Phys. Rev. E 75* (2007), 046109.

[11] Hill, J., Kalkanci, O., McMurry, J. L., and Koser, H. Hydrodynamic surface interactions enable Escherichia coli to seek efficient routes to swim upstream. *Phys. Rev. Lett. 98* (2007), 068101.

[12] Kudrolli, A., Lumay, G., Volfson, D., and Tsimring, L. S. Swarming and swirling in self-propelled polar granular rods. *Phys. Rev. Lett. 100* (2008), 058001.

[13] Lindner, B., and Nicola, E. Critical Asymmetry for Giant Diffusion of Active Brownian Particles. *Phys. Rev. Lett. 101* (2008), 190603.

[14] Narayan, V., Ramaswamy, S., and Menon, N. Long-lived giant number fluctuations in a swarming granular nematic. *Science 317* (2007), 105.

[15] Obata, T., Shimizu, T., Osaki, H., Oshima, H., and Hara, H. Fluctuations in human's walking (II). *J. Korean Phys. Soc. 46* (2005), 713.

[16] Risken, H. *The Fokker-Planck Equation, Methods of Solution and Applications*, 2nd ed. Springer, Berlin, 1989.

[17] Shenoy, V. B., Tambe, D. T., Prasad, A., and Theriot, J. A. A kinematic description of the trajectories of *listeria monocytogenes* propelled by actin comet tails. *PNAS 104* (2007), 8229.

[18] Teeffelen, S., and Löwen, H. Dynamics of a Brownian circle swimmer. *Phys. Rev. E 78* (2008), 020101.

[19] Vicsek, T., Czirók, A., Ben-Jacob, E., Cohen, I., and Shochet, O. Novel type of phase transition in a system of self-driven particles. *Phys. Rev. Lett. 75* (1995), 1226.

[20] Woolley, D. M. Motility of spermatozoa at surfaces. *Reproduction 126* (2003), 259.